Matryoshka-Inspired Micro-Origami Capsules to Enhance Loading, Encapsulation, and Transport of Drugs

Author(s):
Huang, Hen-Wei; Tibbitt, Mark W.; Huang, Tian-Yun; Nelson, Bradley J.

Publication date:
2019-02-13

Permanent link:
https://doi.org/10.3929/ethz-b-000306673

Originally published in:
Soft Robotics 6(1), https://doi.org/10.1089/soro.2018.0028

Funding acknowledgement:
743217 - Soft Micro Robotics (EC)
165564 - Soft Magnetic Robots: Modeling, Design and Control of Magnetically Guided Continuum Manipulators (SNF)

SOFT ROBOTICS
Volume 00, Number 00, 2018

DOI: 10.1089/soro.2018.0028

SoRo
Soft Robotics

Matryoshka-Inspired Micro-Origami Capsules to Enhance Loading, Encapsulation, and Transport of Drugs

Hen-Wei Huang,[1] Mark W. Tibbitt,[2] Tian-Yun Huang,[1] and Bradley J. Nelson[1]

Abstract

Stimuli-responsive hydrogels are promising candidates for use in the targeted delivery of drugs using microrobotics. These devices enable the delivery and sustained release of quantities of drugs several times greater than their dry weight and are responsive to external stimuli. However, existing systems have two major drawbacks: (1) severe drug leakage before reaching the targeted areas within the body and (2) impeded locomotion through liquids due to the inherent hydrophilicity of hydrogels. This article outlines an approach to the assembly of hydrogel-based microcapsules in which one device is assembled within another to prevent drug leakage during transport. Inspired by the famous Russian stacking dolls (Matryoshka), the proposed scheme not only improves drug-loading efficiency but also facilitates the movement of hydrogel-based microcapsules driven by an external magnetic field. At room temperature, drug leakage from the hydrogel matrix is 90%. However, at body temperature the device folds up and assembles to encapsulate the drug, thereby reducing leakage to a mere 6%. The Matryoshka-inspired micro-origami capsule (MIMC) can disassemble autonomously when it arrives at a targeted site, where the temperature is slightly above body temperature. Up to 30% of the encapsulated drug was shown to diffuse from the hydrogel matrix within 1 h when it unfolds and disassembles. The MIMC is also shown to enhance the movement of magnetically driven microcapsules while navigating through media with a low Reynolds number. The translational velocity of the proposed MIMC (four hydrogel-based microcapsules) driven by magnetic gradients is more than three times greater than that of a conventional (single) hydrogel-based microcapsule.

Keywords: hydrogel, microrobotics, reconfigurable structures, controlled drug delivery

Introduction

The integration of stimuli-responsive hydrogels within microrobotic systems has considerable potential for the development of minimally invasive targeted therapies.[1–4] Researchers have made great strides in the development of novel hydrogels that are smaller, safer, softer, and smarter than ever before.[5–11] Research into the stimuli-responsive properties of multilayered structures has made it possible to implement programmable shape transformations to enable the on-demand encapsulation and release of therapeutic agents, including the sustained release of target molecules.[12–15] These structures are also applicable in cardiac microtissue transplantation,[16,17] the microgrippers used in biopsy,[18,19] and cell scaffolds.[20–22] The high water content of hydrogels makes them physically similar to various tissues, thereby ensuring excellent biocompatibility, which facilitates the loading of molecular drugs and responds to external stimuli. Nonetheless, the swelling of hydrogels tends to undermine transport efficiency and accelerate the release of drugs, which mostly promotes drug leakage before reaching targeted sites.[23–25]

The rate of drug release can be moderated by increasing the crosslinking degree within the gel to alter the pore size.[7,26] Unfortunately, most highly crosslinked gels have limited drug-loading capacity and respond slowly to environmental stimuli. Hydrogels with high drug-loading capacity and sustained release can be engineered through the UV polymerization of the mixture of drugs and pregel polymers to trap drug molecules within a densely crosslinked polymer network.[12,27] However, this process is compatible only with drugs that are insensitive to UV light. This method tends to increase the risk that potentially toxic nonpolymerized pregel solutions could diffuse out with the drugs or lead to drug

[1]Institute of Robotics and Intelligent Systems, ETH Zurich, Zurich, Switzerland.
[2]Macromolecular Engineering Laboratory, ETH Zurich, Zurich, Switzerland.

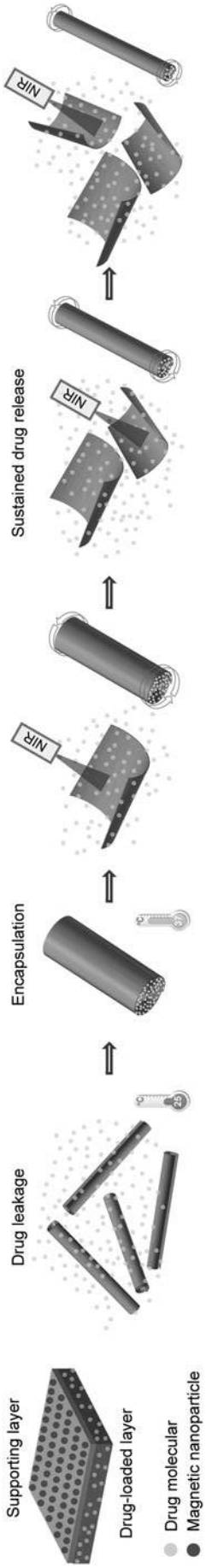

FIG. 1. Schematic of drug leakage from conventional hydrogel bilayer capsules and the drug encapsulation of the MIMC. The MIMC can carry the amount of drug, proportional to the number of assembled hydrogel bilayers, whereas, the amount of leakage is inversely proportional to that. Drug molecules are loaded within the hydrogel matrix of the drug-loaded layer while the pores of the hydrogel network are large at room temperature and then encapsulated by heating the device to body temperature to collapse the polymer networks and refold the microcapsules that shield the drug-loaded layer from the environment. The refolded bilayers are assembled into a single MIMC to further reduce diffusion through the hollow space of the tubular bilayers. Drug delivery is achieved by the unfolding of the microcapsule through exposing NIR light. MIMC, Matryoshka-inspired micro-origami capsule; NIR, near-infrared.

denaturation and aggregation. Furthermore, the low efficiency of the transport process increases the likelihood of leakage. The intrinsically hydrophilic nature of hydrogels induces considerable fluidic drag, which can impede the locomotion of microrobots through media with a low Reynolds number.[28,29] Existing hydrogel-based microrobots suffer from excessive drug leakage during transport to targeted sites or low efficiency with regard to drug loading.[30,31] Finally, the amount of leakage tends to be exacerbated when a swarm of microrobots is used to enhance the overall dose concentration in targeted areas.

In this work, we propose a Matryoshka-inspired micro-origami capsule (MIMC) comprising multiple self-folding hydrogel bilayers. The bilayer structure comprises two hydrogels with different thermal swelling characteristics. The hydrogel that undergoes greater swelling serves as a drug-loading layer, whereas the hydrogel that undergoes less swelling forms a supporting layer with embedded magnetic nanoparticles (MNPs). The embedded MNPs define the folding shape and enable the bilayer to navigate through media using external magnetic fields.[32] The drug is loaded into the drug-loaded layer at room temperature and then encapsulated by heating the device to body temperature. The increase of temperature causes the thermoresponsive hydrogel matrix to collapse, thereby trapping the drug and triggering the self-folded bilayer to refold with the drug-loaded layer shielded from the external environment. Multiple refolded bilayers are subsequently assembled into a single MIMC that inhibits the leakage of the drug from a swarm of hydrogel bilayers (Fig. 1). The MIMC also significantly enhances the transport of hydrogel-based microcapsules through complex biological fluids driven by a magnetic gradient, because the overall magnetic moment of the MIMC is linearly proportional to the number of assembled bilayers. When the MIMC reaches the targeted site (where the temperature is slightly above body temperature), it disassembles autonomously by unfolding the folded bilayers and thereby releases the loaded drug.

Materials and Methods

Preparation of materials used in hydrogel bilayers

We employed a thermoresponsive hydrogel that swells considerably at room temperature and less at the lower critical solution temperature (LCST) as the drug-loaded layer within the self-folding hydrogel bilayer structures. LCST is the transition temperature of thermally responsive hydrogels between the hydrophilic and hydrophobic state. Thermally responsive hydrogels are normally hydrophilic when the temperature is below their LCST. Above the LCST, hydrogels become hydrophobic. Acrylamide (AAm) is added as a hydrophilic comonomer, to make the N-Isopropylacrylamide (NIPAAm) hydrogel more hydrophilic. Therefore, adding acrylamide can enlarge the range of temperature in which the hydrogel is hydrophilic, thus increasing the LCST. NIPAAm was used as the thermoresponsive monomer, and polyethylene glycol diacrylate (PEGDA) was used as a crosslinker. The molar ratio among NIPAAm, AAm, and PEGDA was 90:10:0.5. The photoinitiator 2,2-dimethoxy-2-phenylacetophenone (99%, DMPA) and the solvent ethyl lactate is added at a quantity of 3% and 70% the weight of NIPAAm-AAm-PEGDA, respectively, with the aid of an ultrasonic bath over a period of 20 min.

The supporting layer was composed of NIPAAm, AAm, and PEGDA with a molar ratio of 85:15:2. This composition had a higher LCST and swelled less at room temperature. The photoinitiator and solvent were added in the same proportions as in the drug-loaded layer. Using a probe sonicator (4000 mJ; SONICS), 30 nm MNPs of amorphous Fe_3O_4 (nanostructured and coated with PVP) were dispersed in the supporting layer pregel solution at 0.5 vol%.

Fabrication of hydrogel disk patch

We prepared thermoresponsive hydrogel disks (diameter of 4 mm and thickness of 700 μm) to analyze the swelling properties, drug-loading capacity, encapsulation performance, and drug leakage of the gel matrix at room temperature and body temperature. The hydrogel disks were made by polymerizing a pregel solution of the drug-loaded layer using UV light (365 nm, 3 mW/cm^2). The polymerization process was conducted with the pregel solution between two glass slides separated by two-stacked cover glass with the thickness of 360 μm. Following polymerization, the chamber was immersed in deionized (DI) water for 1 day. During this period, the hydrogel swelled and detached from the glass slides, whereupon any residual unpolymerized pregel solution diffused out from the polymer matrices. A biopsy punch was then used to cut the hydrogel sheet to a defined diameter.

Fabrication of self-folding hydrogel bilayer

Self-folding hydrogel bilayer structures were fabricated using a two-step backside-exposure photolithography process, as shown in Figure 2. A pregel solution of the supporting layer was first polymerized using the UV light between a glass mask and a 5-μm-thick spacer for 1 min. Before polymerization of the supporting layer, we applied a uniform magnetic field with an amplitude of 10 mT in a planar direction for 1 min to align the MNPs to provide directional reinforcement of stiffness. Thus, the direction of the applied magnetic field determined the folding orientation of the bilayer structures. The spacer was removed after polymerization, whereupon the supporting layers attached to the glass mask due to its affinity for hydrophilic molecules. A pregel solution of the drug-loaded layer was introduced into the space between the photomask and a new 30-μm-thick spacer. The drug-loaded layer (below the supporting layer) underwent polymerization through UV exposure for 2 min. After UV curing, the cell was opened to release the layers attached to the photomask. These folded into tubes when immersed in water at room temperature.

Characterizing hydrogels and self-folding bilayers

The swelling characteristics of the thermoresponsive hydrogels determine the drug-loading capacities and affect the self-folding shapes. These characteristics were characterized by measuring their weight at various temperatures between 22°C and 48°C. The hydrogels of the supporting layer and drug-loaded layer were individually polymerized in the shape of a disk. They were first dried in air to measure their dry weight M_d, and then hydrated in DI water. The individual disks of the supporting layer and the drug-loaded layer were kept in a temperature-controlled water bath (Julabo, Germany) to measure the swollen weight (M_s) with varying temperatures. A weight swelling ratio (WSR) was employed

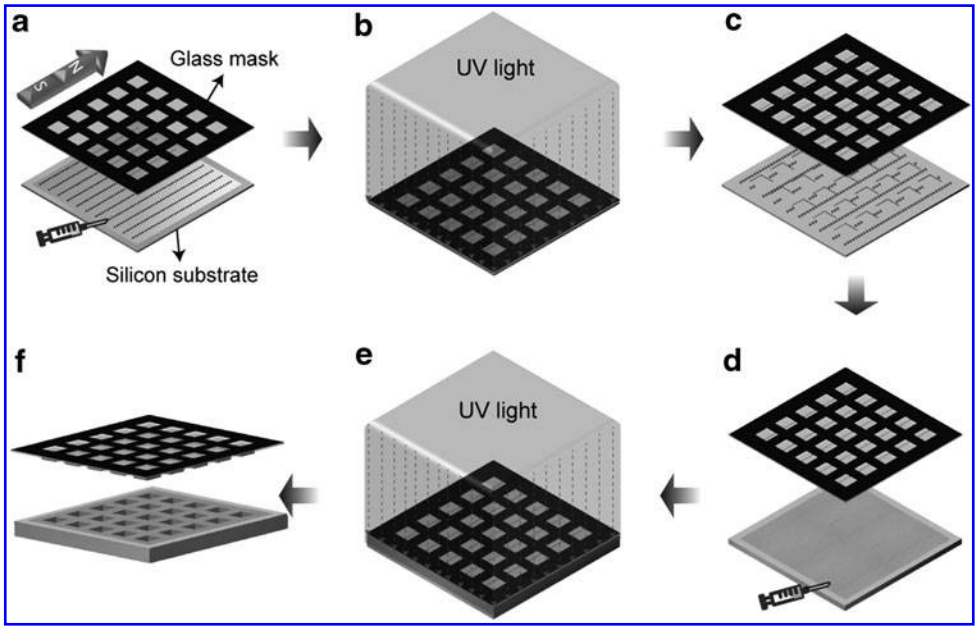

FIG. 2. Schematic illustration showing the process of fabricating hydrogel bilayers: **(a)** applying pregel solution of the supporting layer, in which embedded magnetic nanoparticles were aligned to provide uniaxial reinforcement of stiffness through the application of a homogenous magnetic field; **(b)** photopolymerization of supporting layer using UV light; **(c)** separating the photomask from the silicon substrate (polymerized supporting layers attached to the photomask due to its affinity for hydrophilic molecules); **(d)** a new substrate of greater thickness is filled with pregel solution of the drug-loaded layer; **(e)** UV polymerization of the drug-loaded layer; **(f)** separating the photomask from the substrate. The hydrogel bilayers detach from the mask when immersed in an aqueous solution.

to represent the swelling characteristics of the hydrogels at various temperatures.

$$\mathrm{WSR}(T) = \frac{M_s(T) - M_d}{M_d}. \quad (1)$$

Single degree of freedom shape control of the hydrogel bilayer

Self-folding hydrogel bilayer structures can unfold and refold by increasing the temperature. A modified mathematic model based on Timoshenko bimorph beam theory can be used to estimate the folding curvature of the bilayer structure at various temperatures.

$$\kappa(T) = \frac{6\varepsilon(1+m)^2}{(h_1+h_2)\left(8(1+m)^2 + (1+m\eta)\left(m^2 + \frac{1}{m\eta}\right)\right)} \quad (2)$$

where ε is the difference in expansion coefficient between the supporting layer and drug-loaded layer, h_1 is the thickness of the supporting layer, h_2 is the thickness of the drug-loaded layer, $\eta = \mathrm{E}_1/\mathrm{E}_2$ and $m = h_1/h_2$ are the ratios between the two layers of the elastic modulus and thickness, respectively.

Drug release from hydrogel patch

Gel patches in the shape of a disk were heated up to body temperature to eliminate water from inside the hydrogel. They were then immersed in the model drug solution (Brilliant Green, BG in PBS solution, 1 mM) at room temperature for 24 h. The patches were then removed from the BG solution and immersed in DI water for 5 s to remove residual BG from the surface of the gel disks. The gel disks were immersed in 300 μL of PBS solution within an Eppendorf vessel, whereas the release of the embedded BG from the hydrogel matrices was monitored at room temperature (24°C) and body temperature (37°C) for 1 h. All of the samples were monitored at room temperature for 24 h. We assumed that all of the drug was released from the samples during this period. Every 5 min, PBS solution with released BG was collected, examined using UV-vis spectroscopy (Infinite M200 Pro; Tecan AG, Mannendorf, Switzerland) at a wavelength of 622 nm, and replaced with fresh PBS solution to approximate perfect sink conditions.

FEM simulation of the shape influence on the drug release of self-folded bilayer structures

Simulation conducted by COMSOL Multiphysics® 5.2 was used to elucidate the influence of geometry on molecule diffusion. The physics of transport of diluted species was studied in a time-dependent case. Geometries, such as a square plate, a hollow tube with the drug-loaded layer on the outer side, and a hollow tube with the drug-loaded layer on the inner side, were employed in the solid models.

Drug release from hydrogel bilayers at room temperature

The self-folded hydrogel bilayers were immersed and incubated in a thermostatically controlled water bath at 37°C for 1 min, to dehydrate the drug-loaded layer. The hydrogel bilayers were then removed, and any residual surface water was removed using tissue paper. They were subsequently immersed in a 1-mM BG solution at room temperature and allowed to absorb the model drug over a period of 24 h. They were then immersed in DI water for 1 min to rinse any residual BG from the surface. The bilayers were immersed in 300 μL PBS solution within an Eppendorf vessel, whereas the release of the embedded BG was monitored at room temperature for 24 h. The PBS solution with released BG was collected and replaced with fresh PBS solution every 5 min. The collected solution was examined by UV-vis spectroscopy to analyze the accumulated drug release.

Drug release from hydrogel bilayers at body temperature

The drug-loading process was the same as above; except that, before the hydrogel bilayers were removed from the BG solution, they were heated to 37°C and held at that temperature for 1 h. The bilayers were then removed from the BG solution and immersed in DI water at 37°C to cleanse the residual BG solution and allow the BG solution in the supporting layer to diffuse out for 2 min. The bilayers were then immersed in 300 μL PBS solution at 37°C, while monitoring the release of BG at 37°C for 1 h. The bilayers were then cooled to room temperature, while BG release was monitored for 24 h. Every 5 min, the solution was collected and replaced with fresh PBS solution at 37°C. The accumulated drug release at body temperature was examined in the same way as that at room temperature.

Assembly of MIMCs

The self-folded bilayers are assembled in the model drug solution (BG) at body temperature after the drug is completely loaded into the drug-loaded layer. Heating the device from room to body temperature triggers a transformation in the shape of the self-folded bilayers through unfolding and refolding. Hydrogel bilayers are sequentially transferred into the BG solution at body temperature. The second bilayer is introduced into the BG solution after the first bilayer is completely refolded. The first bilayer is assembled with the second bilayer when the second bilayer refolds. Following the same procedure, the first and second bilayers are assembled with the third bilayer when the third bilayer refolds.

Magnetization of the assembled bilayers

We measured the magnetic hysteresis loops of the MIMC with various numbers of assembled hydrogel-based microcapsules at 302.3 K using a vibrating sample magnetometer (VSM; Oxford Instrument, United Kingdom) under an applied magnetic field in the range of −30 and 30 mT. The MIMCs were glued atop the sample holder of the VSM to fix their shapes.

Magnetic manipulation of the MIMC

Microrobot locomotion was achieved using an eight-coil electromagnetic manipulation system (Octomag)[33] capable of generating a uniform magnetic field of up to 40 mT and magnetic field gradients of up to 1 T/m. A top-view camera was used to observe the scene and record videos of the locomotion process. All experiments were performed in a glass

Petri dish placed in the middle of the workspace, filled with a sucrose solution resembling the viscosity of human blood (approximately 3–4 cP).

Results and Discussion

Hydrogels are composed of a crosslinked polymer network with pores between polymer chains, which allow for diffusion of liquids and solutes. The pore size depends on the types of polymer used to form the network, concentration of crosslinkers, and molecular weight between crosslinks, as well as external stimuli, such as temperature, pH, and electromagnetic fields. The size of the pores determines how drugs diffuse through the hydrogel network by controlling steric interactions between the drugs and the polymer networks. Increasing the density of the crosslinker is the simplest way to reduce the pore size, which in turn reduces the rate of drug leakage. The drug-loading capacity is limited primarily by the highly crosslinked gel matrix.[34] Therefore, the size of the pores is a tradeoff between the drug-loading capacity and the rate of drug release. In this study, we developed a simple yet innovative approach in which hydrogel-based microcapsules are induced to undergo a shape shift and variation of pore size by a change in temperature. This method endows the microcapsule with large drug-loading capacity, strong mechanical strength, and a tunable rate of diffusion.

Single degree of freedom shape control of bilayer structures

Micro-origami capsules with a bilayer structure of two hydrogels with different swelling properties and thermal responses are capable of shape shifting. A bilayer structure comprising two different LCSTs allows the loading, encapsulation, and delivery of drug molecules to be simply controlled by varying temperatures. The drug-loaded layer with the LCST of 37°C dominates shape transformation at temperatures below body temperature, whereas the supporting layer with LCST of 45°C controls shape transformation above body temperature (inset of Fig. 3). The difference in the WSR [Eq. (1)] between the supporting and drug-loaded layer at 25°C induces the bilayer structure to undergo self-folding, wherein the 2D square plate transforms into a hollow tubular shape. In this configuration, the supporting layer is on the inner side of the tube, and the drug-loaded layer is on the outside, which is designed for loading drugs. An increase in temperature decreases the difference in WSR between the two layers, thereby triggering the bilayers to unfold. At 32°C, the bilayer unfolds entirely and then begins to refold in the opposite direction, due to the fact that the WSR of the drug-loaded layer drops to below that of the supporting layer. At 37°C, the bilayer refolds completely, whereas the hydrogel matrix of the drug-loaded layer entirely collapses. In the refolded configuration, the drug-loaded layer is largely shielded from the environment by the supporting layer, which in turn encapsulates the drugs. As the temperature continues to increase from 37°C, the supporting layer gradually dehydrates, triggering the unfolding of the refolded bilayer. At 45°C, the supporting layer entirely dehydrates, and the bilayer fully unfolds, which enables the drug delivery at targeted sites. The corresponding folding curvature of the bilayer is obtained by Equation (2) and shown in Figure 3.

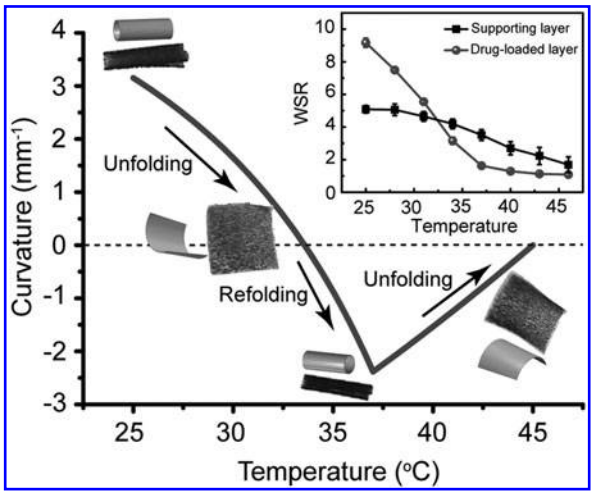

FIG. 3. Calculated curvature of the thermo-responsive hydrogel bilayer versus temperature variations. The *inset* shows the difference in WSR between supporting layer and drug-loaded layer versus temperature variation. WSR, weight swelling ratio.

Drug loading and encapsulation in gel matrix

We selected a model drug (BG) with a molecular size smaller than the pore size of the hydrogels to determine the effects of drug diffusion on the microcapsule with various configurations. Before studying the drug diffusion from the micro-origami capsule, we first investigated the diffusion rate from a bulk gel with the same material composition as the drug-loaded layer by varying the temperature. The BG was shown to diffuse rapidly at 25°C, with the result that more than 90% of the drug molecules diffused from the hydrogel disk within 1 h (Fig. 4). At temperatures below the LCST, the hydrogel is in the swollen state, such that no significant steric interaction occurs between the drug and the matrix. When the temperature exceeds the LCST (37°C), the matrix collapses, resulting in steric interactions during diffusion, which delays the release of drug molecules. At temperatures above 37°C, less than 30% of the BG is released from the hydrogel matrix, which means that more than 70% of the BG can be encapsulated in the hydrogel matrix at body temperature. With a collapsed hydrogel matrix, an increase in temperature has no

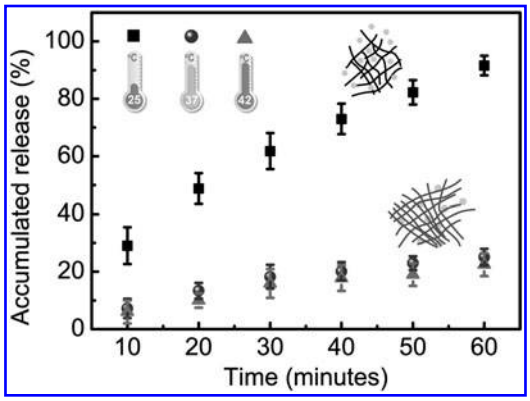

FIG. 4. Accumulated release of BG from the disk-shaped hydrogel patch over time at 25°C, 37°C, and 42°C.

effect on the release of BG from the hydrogel disks. As shown in Figure 4, we observed no difference in the accumulated release of BG between 37°C and 42°C.

Shape influence on drug release

The shape of self-folded microstructures influences their drug release characteristics.[13] We employ the difference in the diffusion of molecules for different shape configurations to implement drug loading, encapsulation, and delivery through a temperature-controlled shape-morphing microcapsule. Figure 5a–c shows the simulation results of the molecule diffusion from the drug-loaded layer to the environment for different configurations. Three configurations of the microcapsules, folded tube, refolded tube, and unfolded plate, are analyzed. The folded tube with the drug-loaded layer on the outer side, designed to absorb the drug solution, allows the molecules to leak into the environment (Fig. 5a). The refolded tube with the drug-loaded layer on the inner side is designed to encapsulate the drug and prevents leakage (Fig. 5b). The unfolded plate, designed to release the encapsulated drug molecules at targeted sites, exhibits unidirectional drug release (Fig. 5c).

Our next step is to investigate the accumulated release of BG from a hydrogel bilayer with various configurations by changing the temperature. At 25°C, nearly 70% of the BG was released from the self-folded bilayer within 1 h (Fig. 5d). The discrepancy in accumulated release between the self-folded tube and the hydrogel disk can be attributed to the overlapping of the drug-loaded area by the supporting layer. When the temperature was increased to 37°C, only 10% of the BG was released by the drug-loaded layer due to the effects of shielding by the supporting layer in the refolded configuration. At body temperature, drug encapsulation is due to the collapse of the hydrogel matrix and the shielding effect. Unlike the hydrogel disk in which an increase of temperature above 37°C has no effect on drug release, accumulated release from the refolded bilayer can be increased to 30% by unfolding the refolded configuration at 42°C. We can employ the increase of drug release by unfolding the shape to deliver the drug at a targeted location by slightly increasing the temperature above the body temperature.

Figure 5d shows that the diffusion of drug molecules from a fully collapsed hydrogel matrix in a bilayer structure can be moderated by changing the configuration to regulate the diffusion length of drug molecules between the gel matrix and the environment. We believe that the 10% leakage from the refolded tube could be reduced further by shielding the hollow space of the tubular bilayer. The assembly of multiple refolded tubes to fill the hollow space could impede diffusion through the hollow space from individual tubes. In this way, it would be possible to reduce leakage from a swarm of devices. Figure 6a presents a comparison of the accumulated release of BG at body temperature between the three refolded tubes and the single MIMC assembled with three cells. The Matryoshka configuration was shown to reduce overall leakage from the bilayers to less than 6% at body temperature. The drug delivery of the MIMC involves unfolding the bilayers to disassemble the MIMC at 42°C (Fig. 6b). Bilayer unfolding can also be actively controlled by an external user by applying a near-infrared (NIR) light. Our previous work shows that the embedded MNPs in the hydrogel can absorb and convert the NIR into temperature elevation to regulate the shape of self-folded microrobots.[32] A location of interest targeted with a NIR light could facilitate autonomous targeted drug delivery using the MIMC shape-morphing microrobots.

Comparing several kinetic models to our accumulated release data, we observe that our results best fit a first-order kinetic model (Supplementary Fig. S1; Supplementary Data are available online at www.liebertpub.com/soro). First-order

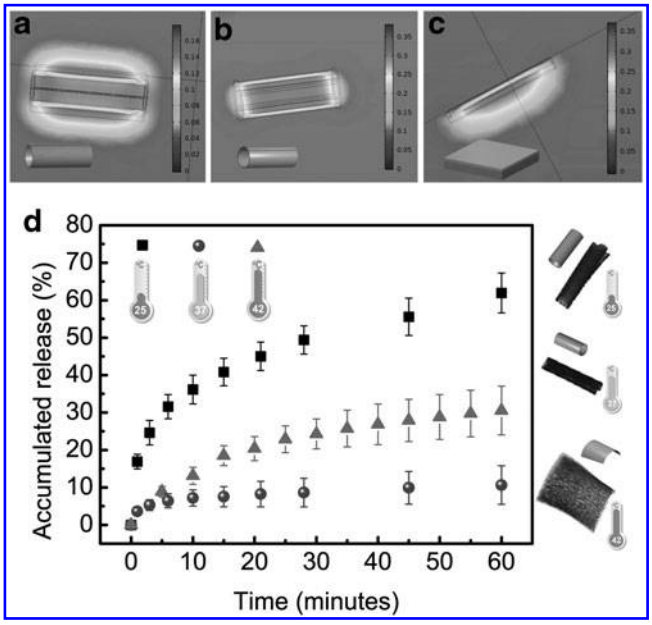

FIG. 5. FEM results of the drug release from the micro-origami capsule at **(a)** 25°C, **(b)** 37°C, and **(c)** 42°C. **(d)** Experimental results of the accumulated drug release from the micro-origami capsule over time with varying the temperature.

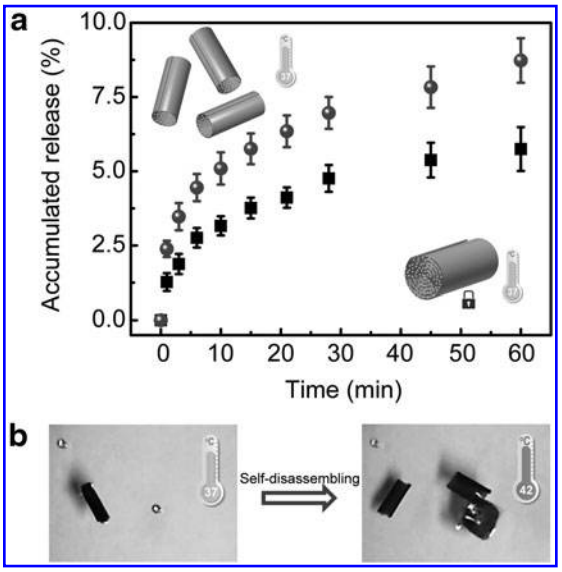

FIG. 6. Encapsulation and delivery of drugs by MIMC: **(a)** comparison of accumulated drug release by hydrogel bilayer tubes and MIMC assembled by three bilayers; **(b)** self-disassembly of MIMC by increasing temperature from 37°C to 42°C.

kinetics is commonly associated with diffusion-controlled polymer matrix systems based on the assumption that the dye or drug is uniformly distributed within the polymer network. However, the first-order kinetic model can only capture the diffusion of drug molecules from polymer networks. In this study, the bilayer structures employ the geometric shielding to achieve drug encapsulation at 37°C. Therefore, the first-order kinetic model cannot fit the diffusion of the bilayer with encapsulated drug molecules. This also suggests that the release is controlled not only by diffusion in the bilayer but also by geometric constraints of the reconfigurable shapes. The widely varying diffusion rate constants shown in Supplementary Table S1 explain the different rates of elution affected by the drug solubility in both the polymer and the drug solution, as well as drug–polymer interactions, diffusivity, and morphology of the polymer network and the folded structures.

Enhanced transport of MIMC

The embedded MNPs control the folding shape and empower the microcapsules to be manipulated wirelessly using magnetic fields to deliver the encapsulated drug to targeted sites in the body. Unfortunately, the intrinsically hydrophilic nature of existing hydrogel-based microrobots hinders their transport. When the tubular microrobot translates and rotates in fluids near a surface, it experiences a drag force and drag torque from the fluid. Both of these values can be estimated by assuming that the microcapsule is a solid circular cylinder rotating and translating along its long axis with a low Reynolds number. The drag force per unit length of a cylinder (L) is defined as follows:

$$F_d/L = \frac{-4\pi\mu_d U}{\ln\left(\frac{2}{k}\right) - \left(\frac{k}{2}\right)^2} \tag{3}$$

where $k = r_c/d_c$, μ_d is the dynamic viscosity of the fluid, and U is the relative velocity between the fluid and the microcapsule. The parameters corresponding to wall interaction are the radius of the cylinder (r_c) and the distance between the center of the microcapsule and the wall (d_c). The drag torque per L of a cylinder rotating close to a wall is given as follows[35]:

$$\tau_d/L = \frac{-4\pi\mu_d\omega_c r_c^2}{\sqrt{1-k^2}} \tag{4}$$

where ω_c is the speed of rotation. To overcome fluidic drag forces, we apply magnetic field H to the microcapsules with flux density $B = \mu_0 H$, where μ_0 is the permeability of vacuum. The magnetic torque that acts on the cylindrical microcapsule can be described as follows[36]:

$$\tau_B = V\mathbf{M}\times\mathbf{B} \tag{5}$$

where $\mathbf{M}$ is the volume magnetization of the object with volume V. The magnetic gradient force acting on the microcapsule is defined as:

$$F_B = V(\mathbf{M}\cdot\nabla)\mathbf{B}. \tag{6}$$

Magnetic manipulation can provide various modes of locomotion, such as translational, rotational, and oscillatory motion, with a high degree of precision.[37] However, the efficiency with which energy of the magnetic field is converted into kinetic energy of the microcapsules is somewhat low, due to considerable fluidic drag and a low concentration of magnetic materials.[32] The proposed Matryoshka-inspired design helps to overcome these difficulties. The magnetic force and torque subjected on microcapsules are both proportional to the magnetic moments ($m = V\mathbf{M}$). Assembling multiple hydrogel bilayers enables a linear increase in the overall magnetic moment in a single MIMC as increasing the number of assembled bilayers (Fig. 7a). The overall magnetic moment of the MIMC can be described as follows:

$$\mathbf{m}_n = \sum_{i=1}^{n} \mathbf{M}_i \cdot V_i. \tag{7}$$

Combining Equations (3) and (6), the translational velocity of the MIMC driven by magnetic gradients can be expressed as follows:

$$U = \frac{\ln\left(\frac{2}{k}\right) - \left(\frac{k}{2}\right)^2}{4\pi\mu_d L}(\mathbf{m}_n \cdot \nabla\mathbf{B}). \tag{8}$$

The geometry and the magnetic moments of the MIMC dominate the translational velocity. When we enhance the magnetic moment by increasing the number of assembled microcapsules, we also enlarge the radius of the MIMC (Fig. 7b), thereby increasing additional drag during locomotion. To elucidate how the number of assembled bilayers

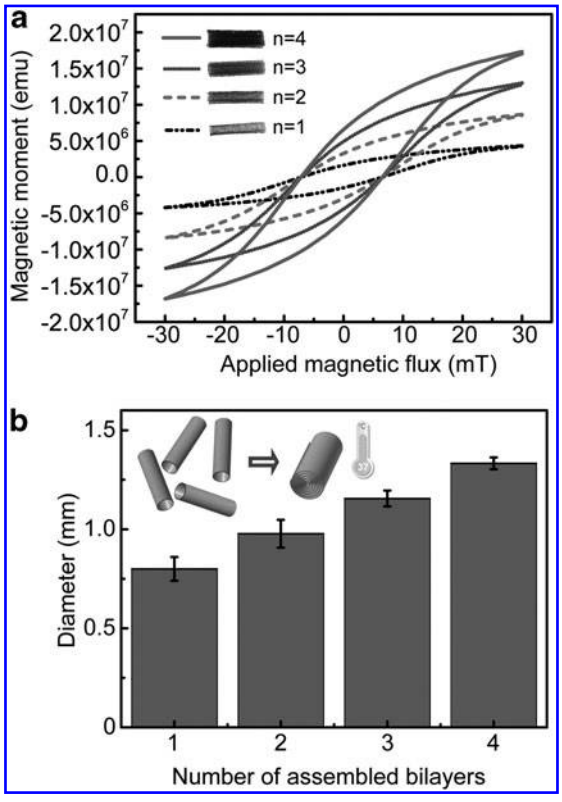

FIG. 7. **(a)** Magnetic hysteresis loops of MIMC assembled with various numbers of bilayers; **(b)** diameter of MIMC versus number of assembled bilayers.

affects translational velocity, we applied a force of 0.2 T/m at 20 mT to move the MIMCs along a predefined linear trajectory. Figure 8a shows that increasing the number of assembled bilayers can significantly speed up the MIMC under the same magnetic field. The velocity of the MIMC with four assembled bilayers was 200% higher than a conventional microcapsule (Fig. 8b). We also examined the rotational motion of the MIMC with various number of assembled bilayers through the application of a rotating magnetic field with the same amplitude (20 mT) but without a gradient. We obtained the highest rotational speed when the MIMCs became desynchronized with the applied rotating magnetic field. Combining Equations (4) and (5), the maximum rotational speed of the MIMC rotating near a surface can be described as follows:

$$\omega_c = \frac{\sqrt{1-k^2}}{4\pi\mu_d \omega r_c^2 L}(\mathbf{m}_n \times \mathbf{B}). \quad (9)$$

Rotational speed is far more sensitive to the geometry of the MIMC than is translational velocity. Any increase in the radius of the MIMC greatly increases drag torque and inhibits rotational speed. The amplification of magnetic torque in the MIMC is mostly compensated for by the increase in fluidic drag torque. Figure 9a shows that increasing the number of assembled microcapsules does not lead to a significant increase in rotational velocity. Nevertheless, translational velocity caused by rolling near a surface can be enhanced by an increase in the radius of the MIMC under nonslip conditions. Figure 9b presents a comparison of translational velocity between a four bilayer MIMC and a conventional microcapsule. These MIMCs were rotated at 1 Hz to avoid slipping across the surface. An increase in the radius of the MIMC can enhance the translational velocity over a surface induced by rolling motion at a relatively low rotating frequency. When the rotating frequency is increased, slippage tends to slow the translation motion. Figure 9c shows the translational motion of the microcapsules rolling over a surface driven by a rotating magnetic field at 3 Hz. The translational velocities of the MIMC and the conventional microcapsule are nearly the same due to slippage at high rotating speed.

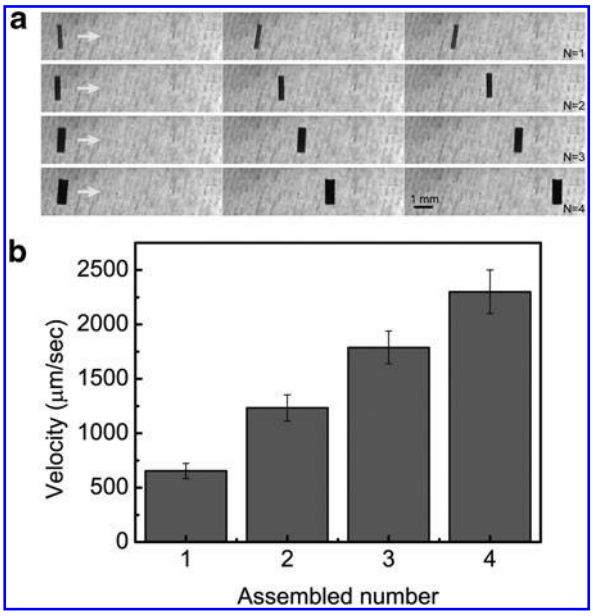

FIG. 8. Translational movement of MIMC driven by magnetic gradients: **(a)** optical images of MIMCs assembled with various numbers of bilayers moving along their long axis; **(b)** measured translational velocity of MIMC versus number of assembled bilayers.

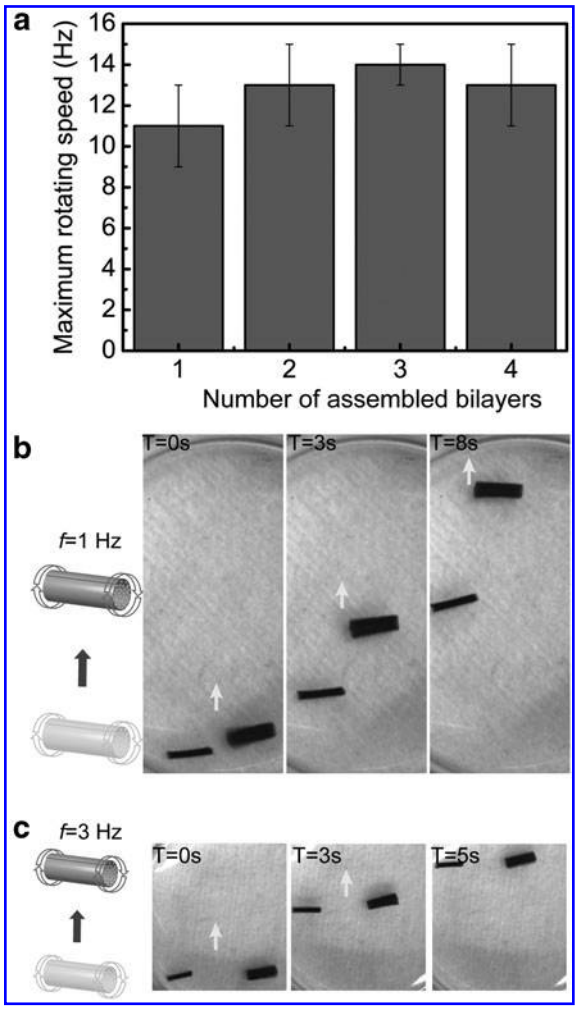

FIG. 9. Rotational motion of MIMC near a surface driven by rotating magnetic field with the amplitude of 20 mT: **(a)** maximum rotating speed of MIMC versus number of assembled bilayers; **(b)** comparison of translational motion of MIMCs of various diameters rolling over a surface at 1 Hz under nonslippage conditions and **(c)** at 3 Hz with MIMCs slipping on the surface.

Conclusions

In this study, we proposed a Matryoshka-inspired assembly of multiple self-folding hydrogel bilayers within a single microcapsule. Our aim was to overcome the severe drug leakage normally associated with hydrogels as well as the enormous fluidic drag forces that hinder their movement through the body. The drug was loaded into a highly swollen hydrogel of a bilayer structure at room temperature and encapsulated at body temperature by entirely collapsing the

hydrogel network and refolding the bilayer. This refolding process encapsulates the drug, such that nearly 90% of the drug can be retained for at least an hour. Multiple hydrogel bilayers are then assembled to form a MIMC with the aim of inhibiting diffusion from the hollow space of the individual folded tubes. In these conditions, less than 6% of the drug diffuses from the MIMC over a period of 1 h. We also sought to enhance transport of the hydrogels by increasing the magnetic moment of the MIMC, which is linearly proportional to the number of assembled hydrogel bilayers. The MIMC design demonstrated improved efficiency with regard to translational motion driven by magnetic field gradient. The translational velocity of the proposed MIMC is $\sim$200% higher than that of a conventional single-device microcapsule.

Acknowledgments

This work was financially supported by the European Research Council Advanced Grant SOMBOT (743217) and the Swiss National Science Foundation (No. 200021_165564). The authors are thankful to Jonathan Perraudin and Soomin Lee for helping in the experiments of drug delivery, to Dr. Salvador Pané for discussions, and the FIRST laboratory of ETH Zurich for technical support.

Author Contributions

H.-W.H. and B.J.N. conceived the ideas and designed the study, H.-W.H. and T.H. performed the experiments, H.-W.H. and M.W.T. analyzed data, and all authors together wrote the article.

Author Disclosure Statement

No competing financial interests exist.

References

1. Nelson BJ, Kaliakatsos IK, Abbott JJ. Microrobots for minimally invasive medicine. Annu Rev Biomed Eng 2010; 12:55–85.
2. Li J, Esteban-Fernández de Ávila B, Gao W, *et al.* Micro/nanorobots for biomedicine: delivery, surgery, sensing, and detoxification. Sci Robot 2017;2:eaam6431.
3. Banerjee H, Ren H. Optimizing double-network hydrogel for biomedical soft robots. Soft Robot 2017;4:191–201.
4. Miyashita S, Guitron S, Yoshida K, *et al.* Ingestible, controllable, and degradable origami robot for patching stomach wounds. In: IEEE International Conference on Robotics and Automation (ICRA), Stockholm, Sweden: IEEE, 2016 May 16–21, pp. 909–916.
5. Wood R, Walsh C. Smaller, softer, safer, smarter robots. Sci Transl Med 2013;5:210ed19.
6. Li J, Mooney DJ. Designing hydrogels for controlled drug delivery. Nat Rev Mater 2016;1:pii: 16071.
7. Hoare TR, Kohane DS. Hydrogels in drug delivery: progress and challenges. Polymer 2008;49:1993–2007.
8. Zhang YS, Khademhosseini A. Advances in engineering hydrogels. Science 2017;356:pii: eaaf3627.
9. Lin S, Yuk H, Zhang T, *et al.* Stretchable hydrogel electronics and devices. Adv Mater 2016;28:4497–4505.
10. Hibbins AR, Kumar P, Choonara YE, *et al.* Design of a versatile pH-responsive hydrogel for potential oral delivery of gastric-sensitive bioactives. Polymers 2017;9:474.
11. Wirthl D, Pichler R, Drack M, *et al.* Engineering instant tough bonding of hydrogels for soft machines and electronics. Sci Adv 2017;3:1–9.
12. Baek K, Jeong JH, Shkumatov A, *et al.* In situ self-folding assembly of a multi-walled hydrogel tube for uniaxial sustained molecular release. Adv Mater 2013;25:5568–5573.
13. Fusco S, Huang HW, Peyer KE, *et al.* Shape-switching microrobots for medical applications: the influence of shape in drug delivery and locomotion. ACS Appl Mater Interfaces 2015;7:6803–6811.
14. Fusco S, Sakar MS, Kennedy S, *et al.* An integrated microrobotic platform for on-demand, targeted therapeutic interventions. Adv Mater 2014;26:533–538.
15. Jeon SJ, Hauser AW, Hayward RC. Shape-morphing materials from stimuli-responsive hydrogel hybrids. Acc Chem Res 2017;50:161–169.
16. Pedron S, Lierop S, Horstman P, *et al.* Stimuli responsive delivery vehicles for cardiac microtissue transplantation. Adv Funct Mater 2011;21:1624–1630.
17. Stuart MAC, Huck WTS, Genzer J, *et al.* Emerging applications of stimuli-responsive polymer materials. Nat Mater 2010;9:101–113.
18. Gultepe E, Randhawa JS, Kadam S, *et al.* Biopsy with thermally-responsive untethered microtools. Adv Mater 2013; 25:514–519.
19. Kuo JC, Tung SW, Yang YJ. A hydrogel-based intravascular microgripper manipulated using magnetic fields. Sens Actuators A Phys 2013;211:1683–1686.
20. Jamal M, Kadam SS, Xiao R, *et al.* Bio-origami hydrogel scaffolds composed of photocrosslinked PEG bilayers. Adv Heal Mater 2013;2:1142–1150.
21. Manikas AC, Aliberti A, Causa F, *et al.* Thermoresponsive PNIPAAm hydrogel scaffolds with encapsulated AuNPs show high analyte-trapping ability and tailored plasmonic properties for high sensing efficiency. J Mater Chem B 2015;3:53.
22. Xu S, Yan Z, Jang KI, *et al.* Assembly of micro/nanomaterials into complex, three-dimensional architectures by compressive buckling. Science 2015;347:154–159.
23. Ionov L. Hydrogel-based actuators: possibilities and limitations. Mater Today 2014;17:494–503.
24. Huang HW, Petruska AJ, Sakar MS, *et al.* Self-folding hydrogel bilayer for enhanced drug loading, encapsulation, and transport. In: Annual International Conference of the IEEE Engineering in Medicine and Biology Society (EMBC), Orlando FL: IEEE, 2016 August 16–20, pp. 2103–2106.
25. Huang HW, Sakar MS, Riederer K, *et al.* Magnetic microrobots with addressable shape control. In: IEEE International Conference on Robotics and Automation (ICRA), Stockholm, Sweden: IEEE, 2016 May 16–21, pp. 2103–2106.
26. Dinarvand R, D'Emanuele A. The use of thermoresponsive hydrogels for on-off release of molecules. J Control Release 1995;36:221–227.
27. Malachowski K, Breger J, Kwag HR, *et al.* Stimuli-responsive theragrippers for chemomechanical controlled release. Angew Chem Int Ed 2014;53:8045–8049.
28. Purcell EM. Life at low Reynolds number. Am J Phys 1977;45:3.
29. Happel J, Brenner H. Low Reynolds Number Hydrodynamics: With Special Applications to Particulate Media. Dordrecht, Netherlands: Springer, 1983.
30. Peters C, Hoop M, Pané S, *et al.* Degradable magnetic composites for minimally invasive interventions: device

fabrication, targeted drug delivery, and cytotoxicity tests. Adv Mater 2016;28:533–538.
31. Breger JC, Yoon C, Xiao R, *et al.* Self-folding thermo-magnetically responsive soft microgrippers. ACS Appl Mater Interfaces 2015;7:3398–3405.
32. Huang HW, Sakar MS, Petruska AJ, *et al.* Soft micromachines with programmable motility and morphology. Nat Commun 2016;7:12263.
33. Kummer MP, Abbott JJ, Kratochvil BE, *et al.* OctoMag: an electromagnetic system for 5-DOF wireless micromanipulation. In: IEEE International Conference on Robotics and Automation (ICRA) 2010 May 3–7, pp. 1610–1616.
34. Fundueanu G, Constantin M, Ascenzi P. Poly(N-isopropylacrylamide-co-acrylamide) cross-linked thermoresponsive microspheres obtained from preformed polymers: influence of the physico-chemical characteristics of drugs on their release profiles. Acta Biomater 2009;5:363–373.
35. Takaisi Y. Note on the drag on a circular cylinder moving with low speeds in a semi-infinite viscous liquid bounded by a plane wall. J Phys Soc Japan 1956;11:1004–1008.
36. Champmartin S, Ambari A, Roussel N. Flow around a confined rotating cylinder at small Reynolds number. Phys Fluids 2007;19:103101–103109.
37. Abbott JJ, Peyer KE, Lagomarsino MC, *et al.* How should microrobots swim? Int J Rob Res 2009;28:1434–1447.

Address correspondence to:
Bradley J. Nelson
Institute of Robotics and Intelligent Systems
ETH Zurich
Zurich 8092
Switzerland

E-mail: bnelson@ethz.ch